DIRECT NUMERICAL SIMULATIONS OF VORTEX SHEDDING BEHIND CYLINDERS WITH SPANWISE LINEAR NONUNIFORMITY

Philippe Parnaudeau, Dominique Heitz
Cemagref,
17, avenue de Cucillé,
F35044 Rennes Cedex - France
philippe.parnaudeau@cemagref.fr
dominique.heitz@cemagref.fr

Eric Lamballais
Laboratoire d'Études Aérodynamiques,
ENSMA, CNRS UMR 6609, Université de Poitiers,
Téléport 2 - Bd. Marie et Pierre Curie B.P. 30179
86962 Futuroscope Chasseneuil Cedex, France
lamballais@univ-poitiers.fr

Jorge H. Silvestrini
Departamento de Engenharia Mecânica e Mecatrônica,
Faculdade de Engenharia,
Pontificia Universidade Catolica do Rio Grande do Sul
Av. Ipiranga 6681, 90619-900 Porto Alegre - RS, Brasil
jorgehs@em.pucrs.br

ABSTRACT

Three-dimensional direct numerical simulations of vortex shedding behind cylinders have been performed when the body diameter and the incoming flow involved spanwise linear nonuniformity. Four configurations were considered: the shear flow, the tapered cylinder and their combination which gave rise to the so called adverse and aiding cases. In contrast with the observations of other investigators, these computations highlighted distinct vortical features between the shear case and the tapered case. In addition, it was observed that the shear case and the adverse case (respec. tapered case and aiding case), yielded similar flow topology. This phenomenon was explained by the spanwise variations of U/D which seemed to govern/characterize these flows. For the cases involving a shear flow a secondary flow was observed, whereas for the tapered cylinder in an uniform flow an singular spanwise velocity component with low magnitude was exhibited. Cellular shedding mode was identified for the four configurations. The taper induced vortex-adhesion points at the location between cells. The lower frequencies of the cells, compared to two-dimensional cylinder in uniform flow, were found to be connected with the oblique vortex shedding.

INTRODUCTION

Three-dimensional vortex shedding is a common feature in many engineering applications such as marine risers, heat exchangers or ultra-clean protection devices in food industry. These complex wake flows usually involve spanwise nonuniformity of the body diameter D and/or of the oncoming flow U. For linear variations of the oncoming flow (constant shear flow) or of the cylinder diameter (linearly tapered cylinder) the flow are considered to be similar in behaviour and exhibit cells of constant frequency, oblique shedding and vortex dislocations (see e.g. Silvestrini & Lamballais (2004); Lamballais & Silvestrini (2002); Mukhopadhyay *et al.* (2002) for shear flows and Piccirillo & Atta (1993); Balasubramanian *et al.* (1998); Vallès *et al.* (2002) for tapered cylinders). Indeed in both cases, U/D and UD can change along the span of the cylinder. Nevertheless, when for a shear flow U/D and UD spanwise distributions are similar, for a tapered cylinder these profiles are opposed. In addition, for linear shear flow the base pressure gradients leads to secondary flow (Woo *et al.*, 1989), whereas for tapered cylinder the base pressure is nearly constant without secondary motion (Vallès *et al.*, 2002). Therefore, the two wakes experience distinct spanwise flow mechanisms. Surprisingly, they are considered to be similar in behaviour (Vallès *et al.*, 2002; Balasubramanian *et al.*, 2001). This viewpoint is mainly explained in the light of the cellular vortex shedding that both flows share. Moreover, when linear nonuniform oncoming flow is combined with linear nonuniform cylinder the wake flows experienced two opposed effects. In one case, in which the maximum velocity corresponds to the large diameter end of the cylinder, the spanwise distribution of UD is enhanced whereas U/D remains constant. In the other case, in which the maximum velocity corresponds to the small diameter end of the cylinder, the spanwise distribution of UD lies in an narrow range whereas U/D is enhanced. Considering the effect of the shear, Balasubramanian *et al.* (2001) explained that in the former case, called the adverse, the shear cancels

the taper, whereas in the latter, called shear aiding taper, the shear aids the taper. In the following we use the name adverse case when the variations of U/D are cancelled, and the name aiding case when they are enhanced.

The aim of this study is to analyse the spanwise dynamical organization and compare the flow topology of the wake behind a circular cylinder in a constant shear flow with the wake of a linearly tapered circular cylinder. Furthermore, in the light of the vortical organisation of these two flows, the responses of the wakes which combine both involved spanwise nonuniformities are investigated. After a short presentation of the four flow configurations considered, some details about the numerical methods are presented. Then, from the vortex visualizations, it is shown that the shear case and the taper case exhibit distinct features, whereas the shear case and the adverse case (respec. tapered case and aiding case), yield similar flow topology. In the three last sections, these observations are discussed from the analysis of the wake transition, secondary flows and frequency variations along the span of the cylinders.

FLOW CONFIGURATION AND PARAMETERS

Uniform and shear flows over circular and tapered cylinder is considered in a Cartesien frame of reference $\Gamma = (0; x; y; z)$, where the cylinder axis is oriented along the vertical direction y at the intersection between the streamwise section x_{cyl} and the spanwise one $z = 0$ (see figure 1). In the case of tapered cylinder, in the interval $-L'_y/2 < y < L'_y/2$, the profile of the diameter $D(y)$, at $x = x_{\rm cyl} = 7D_c$, is given by

$$D(y) = \frac{D_1 + D_2}{2} + \frac{D_2 - D_1}{12}\frac{D_c}{L'_y}\left\{ \ln\left(\frac{\cosh[\frac{6}{D_c}(y + \frac{L'_y}{2})]}{\cosh[\frac{6}{D_c}(y - \frac{L'_y}{2}]}\right)\right\} \tag{1}$$

where $D_c = (D_1 + D_2)/2$ is the median diameter. Outside this interval the diameter is constant and equal to D_1 (for $y < -L'_y/2$) and to D_2 (for $y > L'_y/2$), with $D_1 > D_2$. Note that in the case of circular cylinder the diameter is D_c.

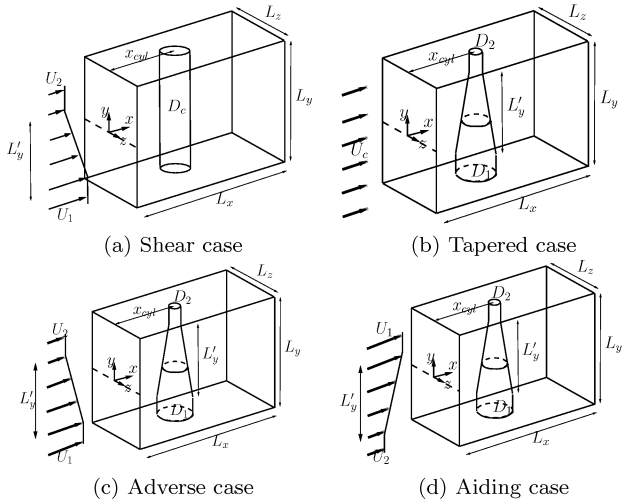

(a) Shear case (b) Tapered case

(c) Adverse case (d) Aiding case

Figure 1: Schematic views of the flow configurations.

At the inflow section, uniform or shear flows are considered. The shear flow is aligned in the y-direction and extended in a zone $-L'_y/2 < y < L'_y/2$. Outside this interval two streams of constant velocities U_1 and U_2 are imposed, with $U_1 > U_2$.

Case	Re_1	Re_2	L'_y	β_U	β_D
Shear	100	300	$40D_c$	0.025	0
Tapered	100	300	$40D_c$	0	0.025
Adverse	100	900	$40D_c$	0.025	0.025
Aiding	150	150	$40D_c$	-0.025	0.025

Table 1: Flow configurations

The inflow velocity profile $U(y)$ at $x = 0$ is

$$U(y) = \frac{U_1 + U_2}{2} + \frac{U_2 - U_1}{12}\frac{D_c}{L'_y}\left\{ \ln\left(\frac{\cosh[\frac{6}{D_c}(y + \frac{L'_y}{2})]}{\cosh[\frac{6}{D_c}(y - \frac{L'_y}{2}]}\right)\right\} \tag{2}$$

without any additional perturbations (steady inflow condition). In the case of a uniform flow, the inflow velocity profile is the median velocity, given by $U_c = (U_1 + U_2)/2$. Note that the shape of the stream velocity is the same as the shape of the cylinder. This shape allows us to consider a constant shear flow extending on a wide region while preserving the free-slip conditions imposed at $y = \pm L_y/2$. As is reported in the paper of Silvestrini & Lamballais (2004), the presence of free-slip walls imposes a kinematic blocking associate with the condition $u_y(x, \pm L_y/2, z) = 0$. Note finally that a periodic boundary condition is imposed in z-direction. The simulations are performed by considering two parameters the shear parameter β_U and the tapered parameter β_D. β_U and β_D are defined by

$$\beta_U = -\frac{D_c}{U_c}\frac{dU}{dy}\ ; \quad \beta_D = -\frac{D_2 - D_1}{L'_y} \tag{3}$$

The couple (β_U, L'_y) and (β_D, L'_y) are considered with $U_1 = 3U_c/2$, $U_2 = U_c/2$ and $D_1 = 3D_c/2$, $D_2 = D_c/2$. The corresponding Reynolds numbers ($Re = U_c D_c/\nu$) is 200 (except in the adverse case where the Reynolds is 400), the variation of the local Reynolds number, associated to the diameter profile (1) and the velocity profile (2) $Re_1 = U_1 D_1/\nu$ and $Re_2 = U_2 D_2/\nu$, are given in the table (1).

The shear flow and the tapered cylinder has the same profile of Reynolds number, ranging from $Re_1 = 300$ to $Re_2 = 100$ along the span of the cylinder. The aiding case has symmetric Reynolds number distribution, with a maximum equal to 200 at midspan, and a minimum equal to $Re_1 = Re_2 = 150$. For the adverse case, the Reynolds number exhibits a parabolic distribution ranging from $Re_1 = 900$ and $Re_2 = 100$.

NUMERICAL METHOD

The incompressible Navier-Stokes equations are directly solved on a Cartesian grid of $n_x \times n_y \times n_z$ points in non-staggered configurations. Sixth-order compact centered difference schemes are used to evaluate all spatial derivatives. Time integration is performed with the second-order Adams-Bashforth scheme. For more details about the numerical code, see Lamballais & Silvestrini (2002). The no-slip condition at the cylinder surface is imposed via an immersed boundary method based on a direct forcing specifically developed to be favourably combined with the use of compact schemes Parnaudeau *et al.* (2003) (see table 2 for additional details on simulation parameters).

Case	Domain	Grid	x_{cyl}
	$L_x \times L_y \times L_z$	$n_x \times n_y \times n_z$	
Forall	$22D_c \times 48D_c \times 12D_c$	$397 \times 385 \times 216$	$7D_c$

Table 2: Parameters of all simulations (Note that the DNS (c) is spatially under-resolved compared with the other calculations).

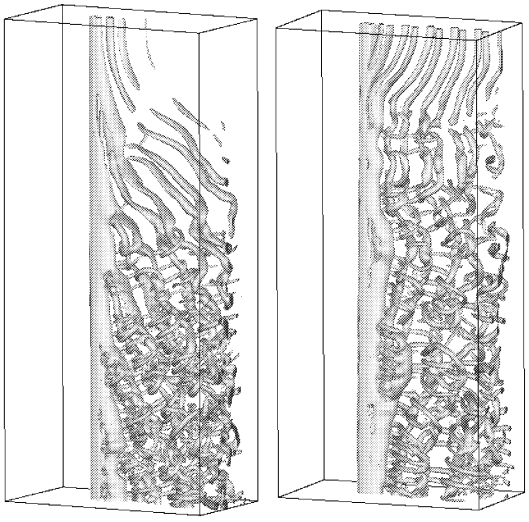

(a) Shear case (b) Tapered case

(c) Adverse case (d) Aiding case

Figure 2: Perspective views showing isosurfaces of the second invariant (Q) of velocity gradient tensor – $Q = 0.2U_c^2/D_c^2$ for $t = 75D_c/U_c$.

RESULTS AND DISCUSSION

Instantaneous vortex pattern

Perspective views of instantaneous isosurfaces of the second invariant $Q = (\Omega_{ij}\Omega_{ij} - S_{ij}S_{ij})/2$ of the velocity gradient tensor are shown in figure 2. The choice of the Q criterion has been made to visualize vortex cores by avoiding the detection of vorticity sheets. It was observed that all flows shared primary von-Kármán vortices, longitudinal vortices, oblique

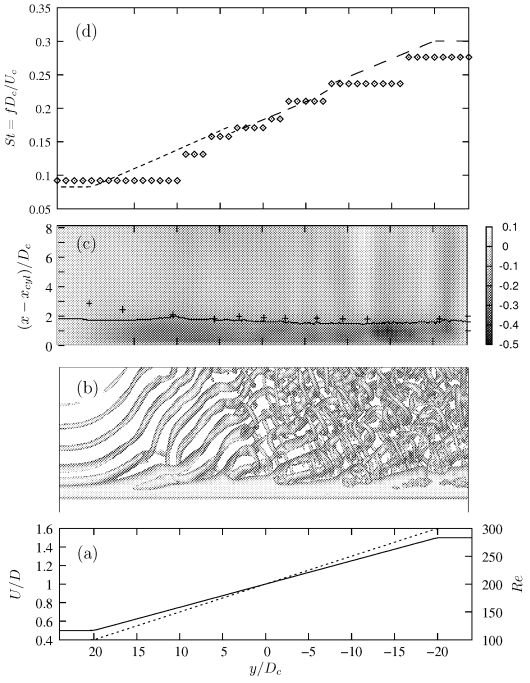

Figure 3: Spanwise distributions in the near wake of the shear case: (a), U/D (–) and Re (- -) ; (b), Instantaneous isosurface of $Q = 0.2U_c^2/D_c^2$ at $t = 75U_c/D_c$; (c), Spanwise mean velocity component (grey level) and formation length (+, Williamson (1996) and Gerrard (1965) measurements), (d); Strouhal number ($\diamond$, present simulations; – –, Fey *et al* (1998) laws).

shedding, and pockets of dislocations[1]. Close examination of figures 3a-b, 4a-b, 5a-b et 6a-b shows that the common feature of the four configurations considered was the connection between the shedding orientation and the sign of the slope of the spanwise distribution of U/D. However, despite the fact that the shear flow configuration and the tapered configuration are considered to be quite similar in behaviour (Vallès *et al.*, 2002; Balasubramanian *et al.*, 2001), the visualizations show that both configurations exhibited distinct features. Furthermore, it was noticed that the shear case and the adverse case (respec. tapered case and aiding case), yielded similar flow topology. Indeed, the shear and adverse flow cases indicated oblique vortex shedding distribution along the span of the cylinder, with increasing slant further downstream. In the very near wake, the angle of the vortex shedding is related to the incoming shear and to the vortex shedding propagation along the span of the cylinder, whereas further downstream the obliqueness is increased by the advection (Silvestrini & Lamballais, 2004). In contrast, the tapered case and the aiding case yielded less regular oblique shedding vortices with spanwise and temporal variations. This phenomenon which may be linked with the large spanwise variations of U/D, leading to large spanwise variations of the vortex shedding frequency, will be discussed in the next sections. In addition, due to the constant spanwise distribution of U/D, the adverse case displayed vortex shedding with large spanwise coherence, compared to the other

[1] Animations (mpeg format) are available on the internet link http://labo.univ-poitiers.fr/informations-lea/tsfp4paper/index.htm

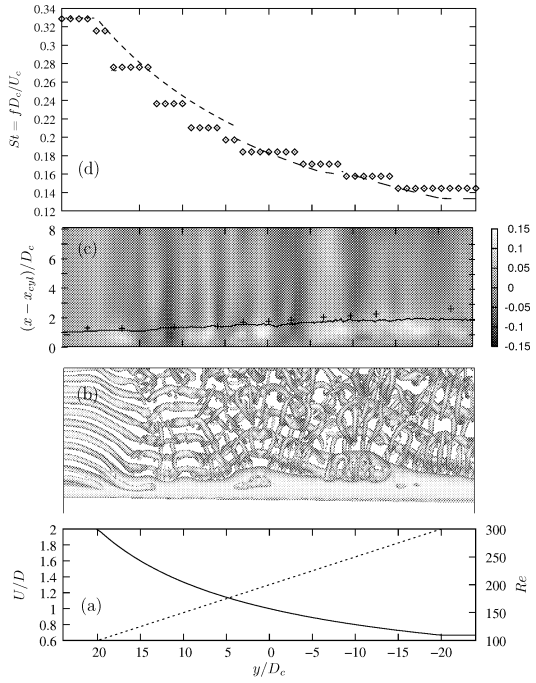

Figure 4: Spanwise distributions in the near wake of the tapered case (see Fig. 3 for details).

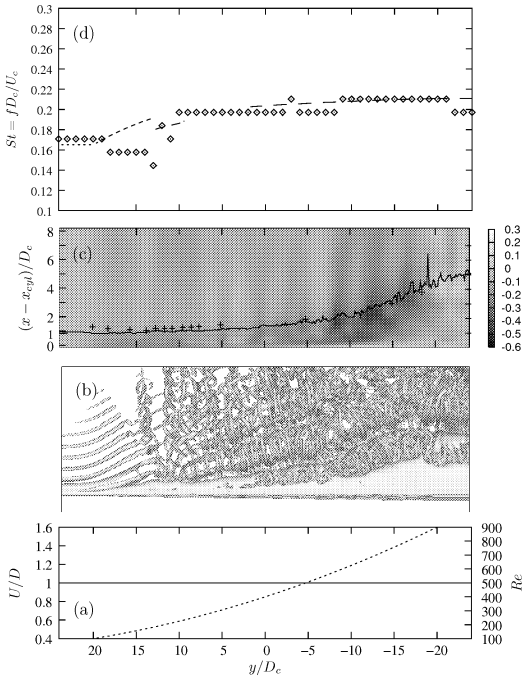

Figure 5: Spanwise distributions in the near wake of the adverse case (see Fig. 3 for details).

configurations which exhibited vortex splitting into cells of approximately constant shedding angle.

Spanwise wake transition

The distributions of Reynolds number associated with the spanwise nonuniformity, of the inflow velocity profile and of the cylinder diameter, are shown in figure 3a, 4a, 5a and 6a.

The wake of two-dimensional cylinders in uniform streams have been extensively studied. For the laminar regime ($50 < Re < 190$) and for the turbulent regime $260 < Re < 5000$, the flow is sensitive to end-conditions and parallel shedding mode can be imposed. Whereas for the wake transition regime ($190 < Re < 250$), the vortex shedding cannot be controlled via boundary manipulations and spontaneous vortex dislocations appear. It is generally considered that the transition to three-dimensionality involves two discontinuities in the Strouhal-Reynolds curve which are linked with two instabilities (Williamson, 1996). The mode A instability, whose onset is about $Re = 190$, is characterized by a spanwise wavelength of about four diameters, associated with streamwise vortices in the Kármán street. The mode B instability, whose onset is around $Re = 230$ and which becomes dominant from $Re = 260$, is characterized by finer scale like streamwise vortices between Kármán vortices with a wavelength of about one diameter. Furthermore, under strong perturbations (i.e. for cylinder with finite aspect ratio in experiments (Williamson, 1992), or strong inhomogeneities in the initial conditions in simulations (Zhang *et al.*, 1995)), vortex-adhesion mode appears for $160 < Re < 230$ and is characterized by spot-like vortex deformations.

In the present flow configurations the aforementioned regimes (laminar, transitional and turbulent) and modes (adhesion, A and B) were identified. Indeed, for the four flows, the three regimes and two of the three modes (vortex-adhesion, A and B) coexisted along the span, and were retrieved at the same Reynolds number values than for uniform wake flow. However, for the case of the tapered and for the case of the aiding, vortex-adhesions appeared more often in time and space along the span of the cylinder than for the two other cases. This mechanisms was responsible of the temporal variations of the oblique shedding angle of the vortices. In figure 5b, for the adverse case, one adhesion points was clearly observed at $y/D_c \simeq 12$ (i.e. in the transitional regime). Interestingly, for the four wake flow considered, adhesion mode appeared even at Reynolds number higher than 230 which is the upper limit for two-dimensional cylinder in uniform flow.

The above general behaviour suggests that the spanwise nonuniformity induced the appearance of vortex-adhesion mode, hence increasing the transition to three-dimensionality. In addition, the diameter taper, or strong spanwise variations of U/D, seemed to enhance this phenomenon. As a result the configurations dominated by the incoming shear flow (i.e. the shear flow and the adverse flow) were not similar in behaviour to those influenced by the taper of the cylinder (i.e. the tapered and the aiding).

Secondary flows and formation length

An important feature of the shear flow is the presence of a secondary flow in the lee side due to the base pressure gradient (Woo *et al.*, 1989; Mukhopadhyay *et al.*, 2002). On the contrary, the wake over a tapered cylinder in a uniform flow, exhibits roughly constant base pressure along the span and no secondary motions have been observed (Vallès *et al.*, 2002).

Figures 3c, 4c, 5c and 6c, show the isovalues of the spanwise mean velocity component. As expected, results indicate that the three configurations which involved a linear incoming

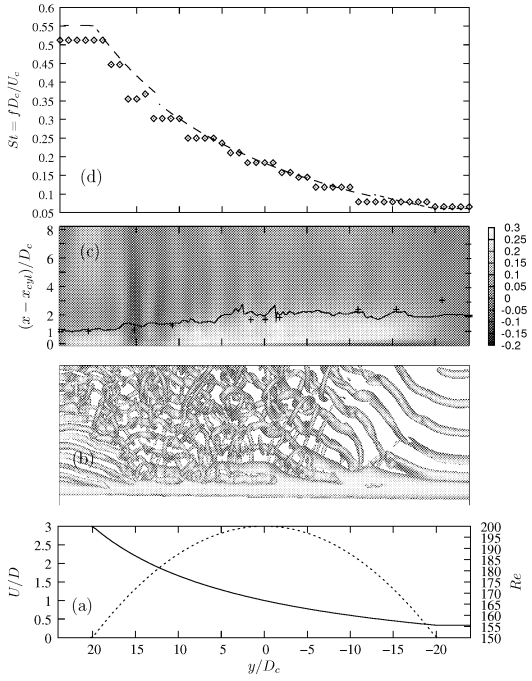

Figure 6: Spanwise distributions in the near wake of the aiding case (see Fig. 3 for details).

velocity profile had a spanwise flow toward the high velocity end. Surprisingly, the tapered cylinder in a uniform flow, yielded a cellular distribution of the spanwise velocity, dominated by cells of motion toward the small diameter end. This wavy distribution of the secondary motions may be related to the three-dimensionalities induced by the adhesion points. Indeed, close examination of the animation showed that the region of reverse spanwise velocity experienced an adhesion-mode. It is also interesting to notice that for the aiding case, an opposite spanwise velocity was also identified in a region with adhesion-mode ($y/D_c \simeq 15$). However, it was worth noting that for the four flow configurations considered, the spanwise secondary motion exhibited wavy distributions. This was explained by the short time integration ($T = 75D_c/U_c$) available to compute the mean velocity. For the cases with nonuniform incoming flow, long time average would give rise to a smooth secondary motion from the low to high velocity end, whereas for the tapered cylinder in a uniform flow we can wonder wether this would still show a dominating secondary motion with low magnitude toward the small diameter end. Indeed in the latter case the direction of the dominating spanwise motion was not explained. At this stage we suggest that it might be induced by the obliqueness of the vortex shedding. This point remains to be explored.

Figures 3d, 4d, 5d and 6d show the spanwise distribution of the formation length. This characteristic length of the near wake formation region was defined as the distance between the cylinder axis and the streamwise coordinate of the points, on each side of the wake, where the r.m.s. of the streamwise velocity has reached a maximum. Results indicate that the secondary flow took place in the recirculation zone. In addition comparisons with the experiments of Williamson (1996) and of Gerrard (1965) showed that the spanwise wake transition influenced the formation length as does the Reynolds

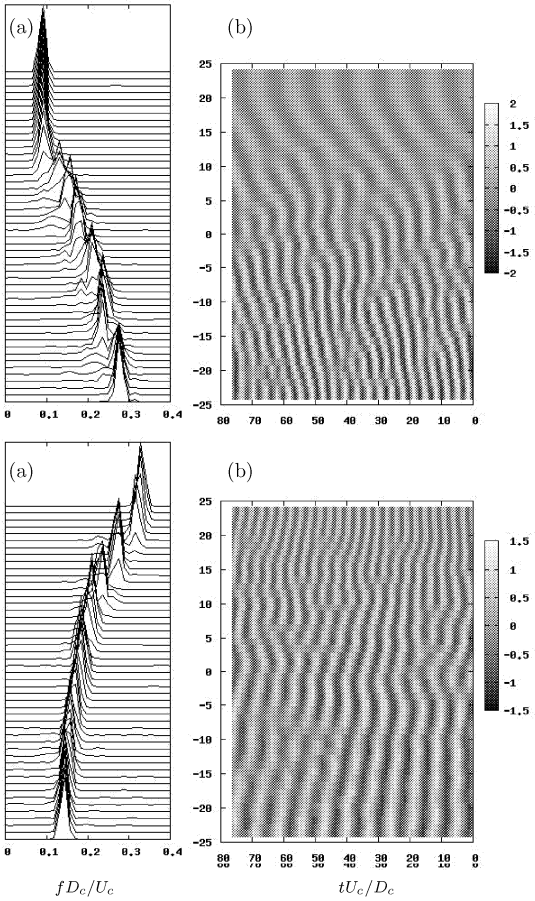

Figure 7: From top to bottom, shear case and tapered case: (a), Spanwise variation of frequency spectra of the transverse velocity component monitored at $(x-x_{cyl})/D_c = 1$ and $z = 0$; (b), Spatiotemporal variations of the transverse velocity along the span of the cylinder.

number for two-dimensional cylinder in uniform flow. Some discrepancies were observed at cylinder end in the side with low values of U/D. This phenomenon, which needs further insight, may be due to an end effect induced by the downward secondary flow.

Frequency analysis

Figures 7a and 8b show the spanwise variation of frequency spectra of the transverse velocity. The spanwise distributions of the Strouhal number, which correspond to the maxima of the spectra, are plotted in figures 3e, 4e, 5e and 6e. For the four cases these frequency distributions scaled on the variation of U/D. However, these distributions were not smooth and the organization of the wakes exhibited cells of constant frequency. Indeed, as already observed in previous studies the cellular pattern of vortex shedding is an adjustment of the vortex shedding frequency to the spanwise nonuniformity. For the adverse case, as there was no variation of U/D, only a single cell was expected. However, results yielded a Strouhal discontinuity corresponding to the spanwise region where the laminar regime gave way to the mode A and mode B regimes. In order to have further insight in the transition of the frequency between cells, spatiotemporal variations of the transverse velocity along the

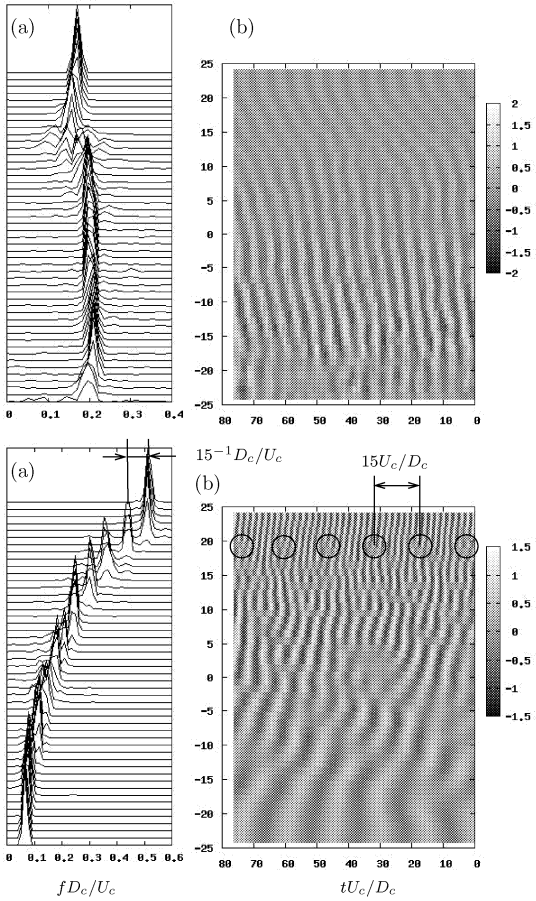

Figure 8: From top to bottom, adverse case and aiding case: See Fig.7 for details.

span of the cylinder are presented in figures 7b and 8b. In these representations the continuous bright region can be considered as the footprints of the vortex line, as there is a link between the maximum of velocity and the passing of the vortices. Results indicated that vortex dislocations appeared at the boundaries of the cells. It is worthwhile to note that the frequency of appearance of the dislocations was equal to the beating frequency of two neighbouring cells. For instance for the aiding case at $y/D_c \simeq 20$ the inverse of the difference of frequency between the two cells $(0.515 - 0.449)^{-1} \simeq 15U_c/D_c$ was nearly equal to the time period measured between two dislocations. At this stage we can easily observe in the region with slight variations of U/D, that much longer time integration would be needed to obtain statistically converged values. Indeed for the adverse and tapered cases only one dislocation can be observed in these spanwise regions. The slope of the time traces of the transverse velocity are equal to the velocity propagation of the vortex shedding along the cylinder. In addition, Silvestrini & Lamballais (2004) suggested that the angle of the vortex shedding is directly link with the characteristic speed of the vortex shedding propagation. Hence our results indicate a spatio-temporal variation of the angle of the vortex shedding around mean values. The mean angles were determined from a scaling of the Strouhal laws, proposed by Fey *et al.* (1998), by the cosine variations along the span. It appeared that the angles found were consistent with the measurements made directly in the views of the instantaneous isosurface of the second invariant (Q). Furthermore, it is observed that in the same spanwise regions where the formation length exhibited singular behaviour (see above), the Strouhal number yielded larger values than for a two-dimensional cylinder in a uniform flow. This phenomenon may be connected with an end effect induced by the secondary flow.

ACKNOWLEDGMENTS

Calculations were carried out at the IDRIS. This study was partially supported by the Région Poitou-Charentes.

REFERENCES

Balasubramanian, S., JR, F. H., Szewczyk, A. & Skop, R. 1998 On the existence of a critical shear parameter for cellular vortex shedding from cylinders in nonuniform flow. *J. Fluids and Structures* **12**, 3–15.

Balasubramanian, S., Jr, F. H., Szewczyk, A. & Skop, R. 2001 An experimental investigation of the vortex-induced vibrations of pivoted tapered circular cylinders in uniform and shear flow. *J. of Wind Engineering and Industrial Aerodynamics* **89**, 757–784.

Fey, U., König, M. & Eckelmann, H. 1998 A new Strouhal-Reynolds-number relationship for the circular cylinder in the range $47 < Re < 2 \times 10^5$. *Phys. Fluids A* **10** (7), 1547–1549.

Gerrard, J. 1965 A disturbance-sensitive Reynolds number range of the flow past a circular cylinder. *J. Fluid Mech.* **22**, 187–196.

Lamballais, E. & Silvestrini, J. 2002 Direct numerical simulation of interactions between a mixing layer and a wake around a cylinder. *J. Turbulence* **3**, 000–028.

Mukhopadhyay, A., Venogopal, P. & Vanka, S. 2002 Oblique vortex shedding from circular cylinder in linear shear flow. *Computer & Fluids* **31**, 1–24.

Parnaudeau, P., Lamballais, E., Heitz, D. & Silvestrini, J. 2003 Combination of the immersed boundary method with compact schemes for DNS of flows in complex geometry. In *Direct and Large-Eddy Simulation V* (ed. R. Friedriech, B. Geurts & O. Métais). Kluwer Academic Publishers.

Piccirillo, P. & Atta, C. V. 1993 An experimental study of vortex shedding behind linearly tapered cylinders at low Reynolds number. *J. Fluid Mech.* **246**, 163–195.

Silvestrini, J. & Lamballais, E. 2004 Direct numerical simulation of oblique vortex shedding from a cylinder in a shear flow. *Int. J. Heat Fluid Flow* **25**, 461–470.

Vallès, B., Anderson, H. & Jenssen, C. 2002 Oblique vortex shedding behind tapered cylinders. *J. Fluids and Structures* **16** (4), 453–463.

Williamson, C. H. K. 1992 The natural and forced deformation of spot-like 'vortex dislocations' in the transition of a wake. *J. Fluid Mech.* **243**, 393.

Williamson, C. H. K. 1996 Three-dimensional wake transition. *J. Fluid Mech.* **328**, 345–407.

Woo, H., Cermak, J. & Peterka, J. 1989 Secondary flows and vortex formation around a circular cylinder in constant shear flow. *J. Fluid Mechanics* **204**, 523–542.

Zhang, H.-Q., Fey, U., Noack, B., König, M. & Eckelmann, H. 1995 On the transition of the cylinder wake. *Phys. Fluids* **7** (4), 779–794.